Parity-doublet bands in the odd-A isotones ^{237}U and ^{239}Pu investigated by a particle-number-conserving method based on the cranked shell model

Jun Zhang [1], Xiao-Tao He [2,*], Yu-Chun Li [3], and Hai-Qian Zhang [2]

[1] *College of Physics, Nanjing University of Aeronautics and Astronautics, Nanjing 210016, China*
[2] *College of Materials Science and Technology, Nanjing University of Aeronautics and Astronautics, Nanjing 210016, China*
[3] *Strategic Technology Equipment Development Center, China Academy of Engineering Physics, Mianyang 621900, China*

(Received 7 October 2022; accepted 24 January 2023; published 10 February 2023)

Based on the reflection-asymmetric Nilsson potential, the parity-doublet rotational bands in odd-A isotones ^{237}U and ^{239}Pu have been investigated by using the particle-number-conserving (PNC) method in the framework of the cranked shell model (CSM). The experimental kinematic moments of inertia (MOIs) and angular momentum alignments are reproduced very well by the PNC-CSM calculations. The significant differences of rotational properties between ^{237}U and ^{239}Pu are explained with the contribution of nucleons occupying proton octupole-correlation pairs of $\pi^2 i_{13/2} f_{7/2}$. The upbendings of MOIs of the parity-doublet bands in ^{237}U are due to the interference terms of alignments of protons occupying $\pi f_{7/2}$ ($\Omega = 1/2$) and the high-j intruder $\pi i_{13/2}$ ($\Omega = 1/2, 3/2$) orbitals. The splittings between the simplex partner bands of the parity-doublet bands in both ^{237}U and ^{239}Pu result from the contribution of alignment of neutron occupying the $\nu d_{5/2}$ ($\Omega = 1/2$) orbital.

DOI: 10.1103/PhysRevC.107.024305

I. INTRODUCTION

The typical feature for octupole correlations in odd-mass nuclei is the appearance of parity-doublet rotational bands, which are pairs of almost degenerate states in excitation energy with the same spin but opposite parities [1–4]. The octupole correlations in nuclei are associated with the single-particle states with orbital and total angular momentum differing by 3, i.e., $\Delta l = \Delta j = 3$ [5,6]. The nuclei with $Z \approx 88$ and $N \approx 134$ in the actinide region are expected to possess the maximum octupole correlations since their proton Fermi surface lies between the proton $f_{7/2}$ and $i_{13/2}$ levels, and neutron Fermi surface lies between the neutron $g_{9/2}$ and $j_{15/2}$ levels [7]. Experimentally, since the first observation of parity-doublet rotational bands in odd-mass ^{229}Pa and ^{227}Ac [8,9], similar bands have been observed in many odd-mass actinide nuclei, like ^{219,223,225}Ac, ^{219,221,223}Fr, ^{221,223}Th, and so on [10–17].

The parity-doublet bands are observed experimentally in ^{237}U and ^{239}Pu, in which some interesting properties are reported [18,19]. In Ref. [18], the angular momentum alignments were compared for the bands in the Pu isotopes with $238 \leqslant A \leqslant 244$, where the sharp backbending observed in the heavier isotopes is not present within the same frequency range in ^{239}Pu. The suddenly gained alignments in the heavier isotopes are due to the contribution from a pair of $i_{13/2}$ protons. There is at present no satisfactory explanation for the absence of backbending phenomenon in ^{239}Pu. As the $N = 145$ isotones closest to the ^{239}Pu, the behavior of the alignments with rotational frequency for ^{237}U is very different. In Ref. [19], a strong backbending in alignment occurs at $\hbar\omega \approx 0.25$ MeV in ^{237}U. In both works, the experimental observations support the presence of the large octupole correlations in the ground states and in the low-lying excited states of odd-A ^{237}U and ^{239}Pu nuclei. The spin and parity are assigned as $K^\pi = 1/2^+$ for the ground-state bands in both nuclei. The experimental data shows that there exist significant simplex splittings at low rotational frequency region in the parity-doublet bands in both nuclei. These issues need further investigations.

Many theoretical approaches were developed to investigate the octupole correlations in nuclei. These include the reflection-asymmetric mean-field approach [20–22], algebraic models [23,24], cluster models [25–27], vibrational approaches [28–30], reflection asymmetric shell model [31–33], and cranked shell model [34–38]. The particle-number-conserving method in the framework of cranked shell model (PNC-CSM) is one of the most useful models to describe the rotational bands [39–41]. In the PNC-CSM calculations, the cranked shell model Hamiltonian is diagonalized directly in a truncated cranked many-particle configuration (CMPC) space. The particle number is conserved exactly and the Pauli blocking effects are taken into account spontaneously. The previous PNC-CSM method has been developed to deal with reflection-asymmetric nuclei, and successfully applied to describe the alternating-parity rotational bands in the even-even nuclei [38].

In this work, the PNC-CSM method is further applied to describe the ground-state parity-doublet rotational bands in odd-A nuclei ^{237}U and ^{239}Pu. The ground-state spin assignments are identified for both nuclei. By considering the octupole correlations, Pauli blocking effects and Coriolis interaction, the striking differences of rotational properties

*hext@nuaa.edu.cn

between ^{237}U and ^{239}Pu and the simplex splittings of the parity-doublet bands in both nuclei are investigated in detail.

A brief introduction of the PNC-CSM method dealing with the reflection-asymmetric nuclei are presented in Sec. II. The detailed PNC-CSM analyses for the parity-doublet rotational bands in ^{237}U and ^{239}Pu are presented in Sec. III. A summary is given in Sec. IV.

II. THEORETICAL FRAMEWORK

The detailed understanding of PNC-CSM method dealing with the reflection-asymmetric nucleus can be found in Ref. [38]. Here we give a brief description of the related formalism. The cranked shell model Hamiltonian of an axially symmetric nucleus in the rotating frame [42–44] is

$$H_{\mathrm{CSM}} = H_0 + H_{\mathrm{P}} = H_{\mathrm{Nil}} - \omega J_x + H_{\mathrm{P}}. \tag{1}$$

$H_{\mathrm{Nil}} = \sum h_{\mathrm{Nil}}(\varepsilon_2, \varepsilon_3, \varepsilon_4)$ is the Nilsson Hamiltonian, where quadrupole (ε_2), octupole (ε_3), and hexadecapole (ε_4) deformation parameters are included. $-\omega J_x = -\omega \sum j_x$ represents the Coriolis interaction with the rotational frequency ω about the x axis (perpendicular to the nucleus symmetry z axis).

When $\hbar\omega = 0$, for an axially symmetric and reflection-asymmetric system, the single-particle Hamiltonian has nonzero octupole matrix elements between different shell N. Since parity $p = (-1)^N$, the parity is no longer a good quantum number, but the single-particle angular momentum projection on the symmetry axis Ω is still a good quantum number. The single-particle orbitals can be labeled with the quantum numbers Ω (l_j), where l_j are the corresponding spherical quantum numbers.

However, when $\hbar\omega \neq 0$, due to the Coriolis interaction $-\omega j_x$, the Ω is no longer a good quantum. Since the reflection through plane yoz, S_x invariant holds [45]. The single-particle orbitals can be labeled with the simplex quantum numbers s ($s = \pm i$), which are the eigenvalues of S_x operator.

The pairing H_{P} includes the monopole and quadrupole pairing correlations $H_{\mathrm{P}}(0)$ and $H_{\mathrm{P}}(2)$,

$$H_{\mathrm{P}}(0) = -G_0 \sum_{\xi\eta} a^\dagger_\xi a^\dagger_{\bar{\xi}} a_{\bar{\eta}} a_\eta, \tag{2}$$

$$H_{\mathrm{P}}(2) = -G_2 \sum_{\xi\eta} q_2(\xi) q_2(\eta) a^\dagger_\xi a^\dagger_{\bar{\xi}} a_{\bar{\eta}} a_\eta, \tag{3}$$

where $\bar{\xi}(\bar{\eta})$ labels the time-reversed state of a Nilsson state $\xi(\eta)$, $q_2(\xi) = \sqrt{16\pi/5}\langle\xi|r^2 Y_{20}|\xi\rangle$ is the diagonal element of the stretched quadrupole operator, and G_0 and G_2 are the effective strengths of monopole and quadrupole pairing interactions, respectively.

By diagonalizing H_{CSM} in a sufficiently large CMPC space, a sufficiently accurate low-lying excited eigenstate is obtained as

$$|\psi\rangle = \sum_i C_i |i\rangle, \tag{4}$$

where C_i is real and $|i\rangle = |\mu_1\mu_2 \ldots \mu_n\rangle$ is a cranked many-particle configuration for an n-particle system, and $\mu_1\mu_2 \ldots \mu_n$ are the occupied cranked Nilsson orbitals. The configuration $|i\rangle$ is characterized by the simplex s_i,

$$s_i = s_{\mu_1} s_{\mu_2} \ldots s_{\mu_n}, \tag{5}$$

where s_μ is the simplex of the particle occupying in orbital μ.

The occupation probability of each cranked orbital μ can be calculated as

$$n_\mu = \sum_i |C_i|^2 P_{i\mu}. \tag{6}$$

Here, $P_{i\mu} = 1$ if μ is occupied and $P_{i\mu} = 0$ otherwise.

The angular momentum alignment of eigenstate, including the diagonal and off-diagonal parts, can be written as

$$\langle\psi|J_x|\psi\rangle = \sum_i |C_i|^2 \langle i|J_x|i\rangle + \sum_{i\neq j} C_i^* C_j \langle i|J_x|j\rangle, \tag{7}$$

and the kinematic moment of inertia is

$$J^{(1)} = \frac{1}{\omega}\langle\psi|J_x|\psi\rangle. \tag{8}$$

For reflection-asymmetric systems with odd number of nucleons [45], the experimental rotational band with simplex s is characterized by spin state I of alternating parity,

$$s = +i, I^p = 1/2^+, 3/2^-, 5/2^+, 7/2^-, \ldots, \tag{9}$$

$$s = -i, I^p = 1/2^-, 3/2^+, 5/2^-, 7/2^+, \ldots. \tag{10}$$

The angular momentum alignment for positive- and negative-parity bands can be expressed as [46]

$$\langle J_x\rangle_p = \langle\psi|J_x|\psi\rangle - \frac{1}{2} p \triangle I_x(\omega), \tag{11}$$

$$J_p^{(1)} = \frac{\langle\psi|J_x|\psi\rangle}{\omega} - \frac{1}{2} p \triangle J^{(1)}(\omega), \tag{12}$$

where $|\psi\rangle$ is the parity-independent wave function with the rotational frequency ω calculated by PNC-CSM method. The $\triangle I_x(\omega)$ and $\triangle J^{(1)}(\omega)$ are parity splitting of the alignment and moment of inertia in the experiment rotational bands, respectively. The corresponding values can be obtained by the following formula:

$$\triangle I_x(\omega) = I_{x-}(\omega) - I_{x+}(\omega), \tag{13}$$

$$\triangle J^{(1)}(\omega) = J_-^{(1)}(\omega) - J_+^{(1)}(\omega), \tag{14}$$

in which $+(-)$ represents the positive- (negative-) parity in the experiment rotational bands.

III. RESULTS AND DISCUSSIONS

A. Parameters

In the present calculation, the values of Nilsson parameters (κ, μ) are taken from Ref. [47]. The deformation parameters ε_2, ε_3, ε_4 are input parameters in the PNC-CSM calculations, the values employed in this work are listed in Table I. The deformation parameters ε_2 and ε_4 for nuclei ^{237}U and ^{239}Pu are taken as an average of the neighboring even-even U ($Z = 92$) and Pu ($Z = 94$) isotopes [38]. The ε_3 values used in this work are chosen by fitting the experimental MOIs and alignments of the ground-state bands in ^{237}U and ^{239}Pu.

TABLE I. Deformation parameters ε_2, ε_3, ε_4 used in the present PNC-CSM calculations for ^{237}U and ^{239}Pu.

	ε_2	ε_3	ε_4
^{237}U	0.210	0.071	−0.045
^{239}Pu	0.230	0.010	−0.055

The effective pairing strengths G_0 and G_2, in principle, can be determined by the odd-even differences in nuclear binding energies, and are connected with the dimensions of the truncated CMPC space. For both ^{237}U and ^{239}Pu, the CMPC space is constructed in the proton $N = 5$, 6 shells and the neutron $N = 6$, 7 shells. The dimensions of the CMPC space are about 1000 for both protons and neutrons. The corresponding effective monopole and quadrupole pairing strengths are $G_{0p} = 0.25$ MeV and $G_{2p} = 0.03$ MeV for protons, $G_{0n} = 0.15$ MeV and $G_{2n} = 0.01$ MeV for neutrons. In this work, the same values of effective pairing parameters are used for ^{237}U and ^{239}Pu. The stability of the PNC-CSM calculations against the change of the dimensions of the CMPC space has been investigated in Ref. [39].

B. Cranked Nilsson levels

Figures 1 and 2 show the cranked Nilsson levels near the Fermi surface of ^{237}U and ^{239}Pu, respectively. Due to the octupole correlations, the single-particle orbitals are parity-mixed, the only conserved quantum numbers is Ω, which represents the projection of the single-particle total angular momentum j on the symmetry axis. So the parity-mixed proton and neutron orbitals are labeled by quantum number Ω at the band head ($\omega = 0$), and the simplex $s = +i$ ($s = -i$) levels are denoted by solid (dotted) lines. For both protons and neutrons, such sequences of single-particle levels are found to be reasonable in agreement with experimental data taken from Refs. [48,49]. The $Z = 92$, 96 gaps for protons and $N = 150$, 152 gaps for neutrons are presented in nearly all odd-mass actinides, remarkably similar to the results predicted by the Woods-Saxon potential.

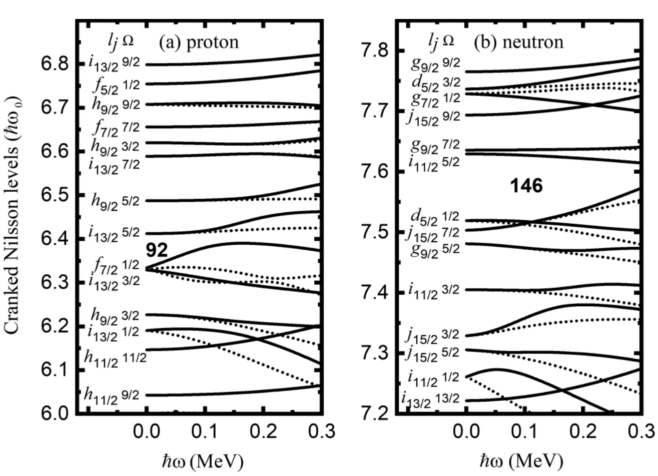

FIG. 1. The cranked Nilsson levels near the Fermi surface of ^{237}U for protons (a) and neutrons (b). The simplex $s = +i$ ($s = -i$) levels are denoted by black solid (dashed) lines.

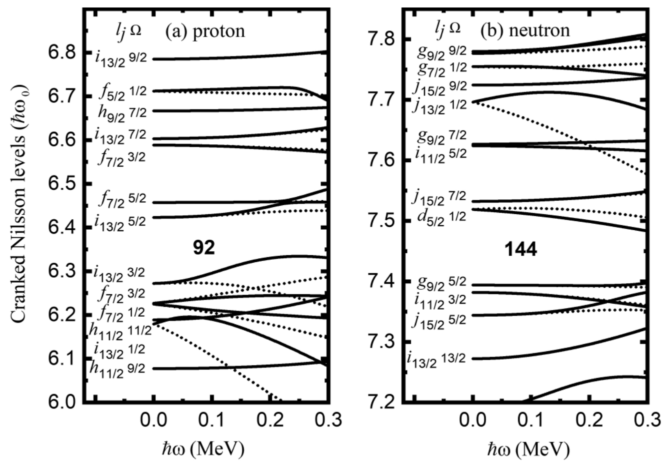

FIG. 2. The same as Fig. 1, but for cranked Nilsson levels near the Fermi surface of ^{239}Pu.

Comparing the proton single-particle levels for ^{237}U and ^{239}Pu, the proton $\Omega = 1/2$ level from $\pi f_{7/2}$ orbital just locates at the Fermi surface for ^{237}U, while it is far below the Fermi surface for ^{239}Pu. As we known, $\pi f_{7/2}$ and $\pi i_{13/2}$ proton orbitals form the basis for the existence of strong octupole correlations in the actinide region. The neutron $\nu 1/2$ ($d_{5/2}$) orbital locates just at the Fermi surface for both ^{237}U and ^{239}Pu nuclei, which are consistent with the experimental ground state configuration with $K = 1/2$.

C. Parity-doublet bands in ^{237}U and ^{239}Pu

Figure 3 shows the experimental and calculated moments of inertia (MOIs) and alignments of the parity-doublet rotational bands in ^{237}U and ^{239}Pu. The experimental data are taken from Refs. [48,49], which are reproduced very well by the PNC-CSM calculations. One can see that the rotational behaviors of the parity-doublet bands in ^{237}U and ^{239}Pu are very different. From Figs. 3(e) and 3(f), there are sharp upbendings at $\hbar\omega \approx 0.25$ MeV for both the $s = +i$ and $s = -i$ alternating-parity bands in ^{237}U. In contrast, as shown in Figs. 3(g) and 3(h), the rotational behaviors are much plainer for bands in ^{239}Pu. It is well known that the backbending is caused by the crossing of the ground-state band with a pair-broken band based on high-j intruder orbitals. In this mass region, the high-j intruder orbitals involved in the Fermi surface are the $\pi i_{13/2}$ and $\nu j_{15/2}$ orbitals.

Figures 4 and 5 show the occupation probability n_μ of each orbital μ (including both $s = \pm i$) near the Fermi surface for the parity-doublet bands in ^{237}U and ^{239}Pu for protons and neutrons, respectively. The Nilsson levels far above ($n_\mu \approx 0$) and far below ($n_\mu \approx 2$) the Fermi surface are not shown. In Fig. 5, the occupation probabilities of neutron orbitals in both $s = +i$ and $s = -i$ bands are almost constant with rotational frequency $\hbar\omega$ increasing, which contribute little to the ω variation of $J^{(1)}$. The different behavior of the rotational bands in ^{237}U and ^{239}Pu would be the result of the contribution from protons.

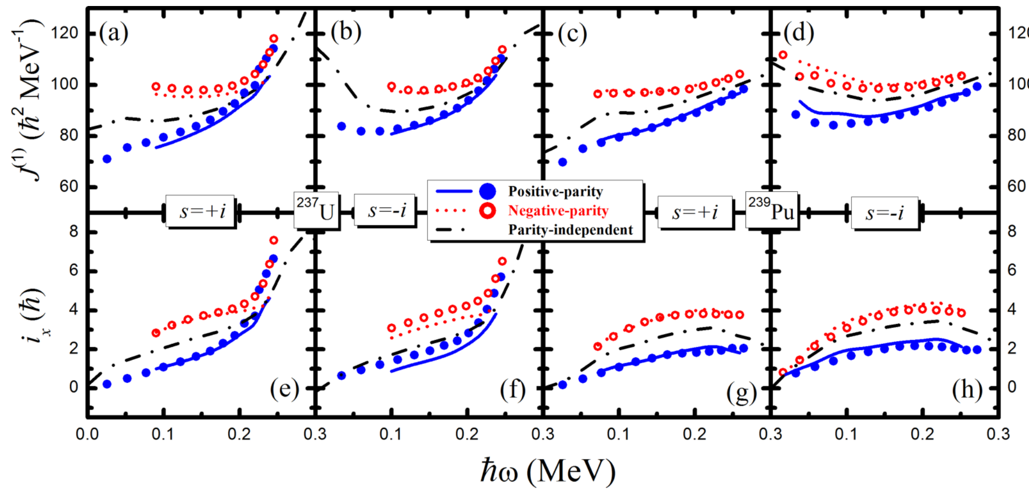

FIG. 3. The kinematic moments of inertia $J^{(1)}$ (top row) and alignments $i_x = \langle J_x \rangle - \omega J_0 - \omega^3 J_1$ (bottom row) of the parity-doublet rotational bands in ^{237}U and ^{239}Pu. The Harris parameters are adopted as $J_0 = 65\hbar^2$ MeV^{-1} and $J_1 = 369\hbar^4$ MeV^{-3}. The experimental data are denoted by blue solid and red open circles for the positive- and negative-parity bands, respectively. The PNC-CSM calculations of parity-independent bands are denoted by dash-dotted lines. After considering the parity splitting of Eqs. (14) and (13), the positive- and negative-parity bands are denoted by blue solid and red dotted lines, respectively.

From Fig. 4(a), it can be seen that the occupation probabilities of proton orbitals $\pi 1/2$ ($f_{7/2}$), $\pi 3/2$ ($i_{13/2}$) are almost constant ($n_\mu \approx 1.5$) at $\hbar\omega < 0.25$ MeV and increase slowly at $\hbar\omega > 0.25$ MeV. The occupation probability of orbital $\pi 5/2$ ($i_{13/2}$) drops down gradually from one to nearly zero from about 0.25 MeV to 0.30 MeV. The occupation of proton orbitals $\pi 1/2$ ($f_{7/2}$), $\pi 3/2$ ($i_{13/2}$), and $\pi 5/2$ ($i_{13/2}$) leads to the upbending of proton alignment at $\hbar\omega \approx 0.25$ MeV for the parity-doublet bands in ^{237}U [see Fig. 6(c)].

For ^{239}Pu, the proton occupation probability of high-j intruder orbital $\pi 5/2$ ($i_{13/2}$) increases slightly at $\hbar\omega < 0.20$ MeV and decreases slightly at $\hbar\omega > 0.20$ MeV. The occupation probability of orbital $\pi 5/2$ ($f_{7/2}$) decreases slowly at $\hbar\omega < 0.20$ MeV and slow increase at $\hbar\omega > 0.20$ MeV. These lead to the angular momentum alignments keep nearly constant at $\hbar\omega < 0.20$ MeV and slowly decrease at $\hbar\omega > 0.20$ MeV in the parity-doublet bands in ^{239}Pu [see Figs. 3(g) and 3(h)].

In order to clearly understand the upbending mechanism, the contributions of protons to the angular momentum alignments $\langle J_x \rangle$ in the parity-doublet bands in ^{237}U and ^{239}Pu are shown in Fig. 6. Figure 6(a) shows that the sharp increase for the parity-doublet bands in ^{237}U mainly comes from the off-diagonal part of proton alignments. However, as shown in Fig. 6(b) that both the diagonal and off-diagonal parts vary smoothly for the rotational bands in ^{239}Pu.

The contribution of interference terms $j_x(\mu\nu)$ between the proton orbitals μ and ν to the off-diagonal angular momentum alignments in the parity-doublet bands in ^{237}U and ^{239}Pu are

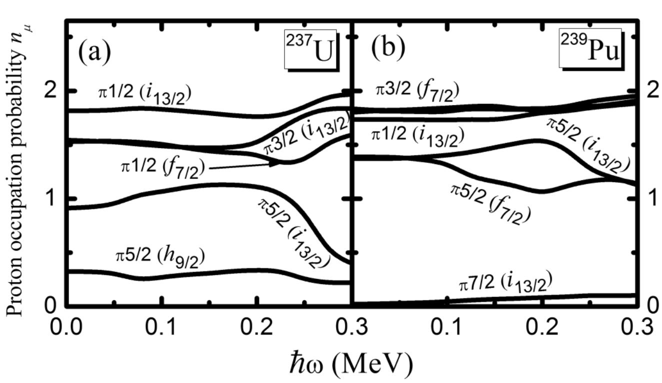

FIG. 4. The occupation probability n_μ of each orbital μ (include both $s = \pm i$) for protons near the Fermi surface for the parity-doublet bands in ^{237}U and ^{239}Pu. The Nilsson levels far above ($n_\mu \approx 0$) and far below ($n_\mu \approx 2$) the Fermi surface are not shown.

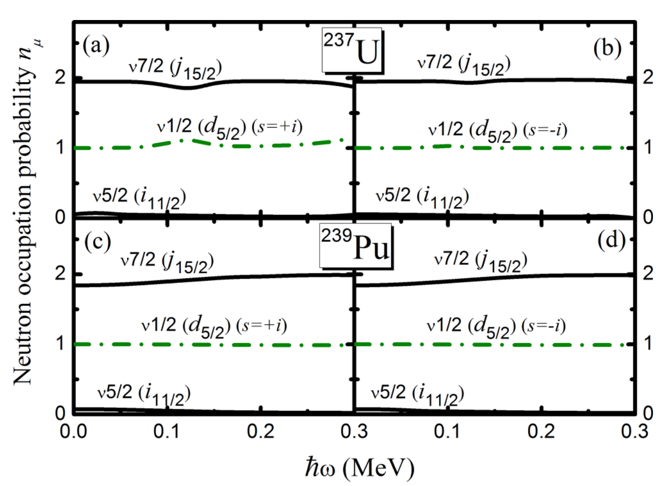

FIG. 5. The occupation probability n_μ of each orbital μ (include both $s = \pm i$ unless otherwise specified) for neutrons near the Fermi surface for the parity-doublet bands in ^{237}U (top row) and ^{239}Pu (bottom row). The Nilsson levels far above ($n_\mu \approx 0$) and far below ($n_\mu \approx 2$) the Fermi surface are not shown.

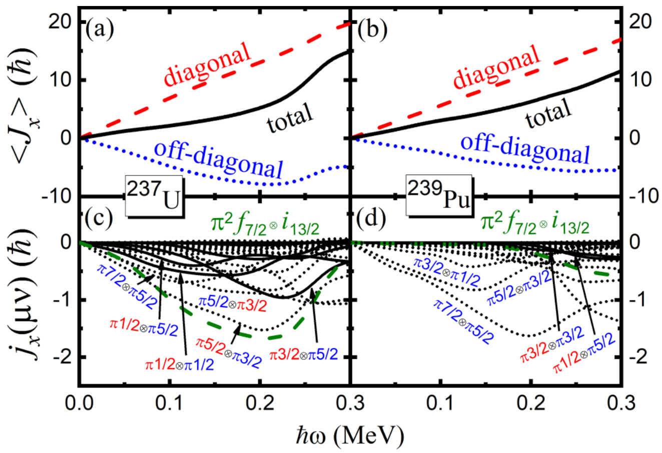

FIG. 6. Contributions of protons to the angular momentum alignments $\langle J_x \rangle$ for the parity-doublet bands in ^{237}U and ^{239}Pu. The diagonal $\sum_{\mu} j_x(\mu)$ and off-diagonal parts $\sum_{\mu<\nu} j_x(\mu\nu)$ are denoted by red dashed and blue dotted lines, respectively (top row). The interference term $j_x(\mu\nu)$ between orbitals from proton $\pi^2 i_{13/2} f_{7/2}$ pairs are denoted by black solid lines, other interference terms are denoted by black dotted lines. The total interference terms from proton $\pi^2 i_{13/2} f_{7/2}$ pairs are denoted by olive dashed lines. Orbitals from $\pi f_{7/2}$ and $\pi i_{13/2}$ are denoted by red and blue quantum numbers Ω, respectively (bottom row).

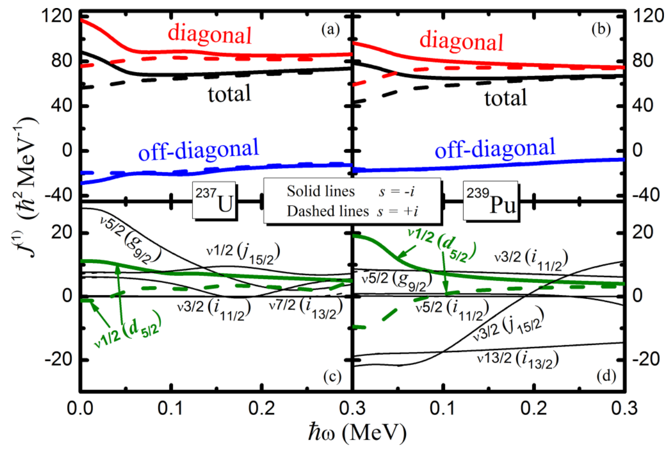

FIG. 7. Contributions of neutrons to the moments of inertia $J^{(1)}$ for the parity-doublet bands in ^{237}U and ^{239}Pu. The diagonal $\sum_{\mu} j_x(\mu)$ and off-diagonal parts $\sum_{\mu<\nu} j_x(\mu\nu)$ are denoted by red and blue lines, respectively (top row). The contribution of nucleon occupying each neutron orbitals are presented in bottom row.

shown in Figs. 6(c) and 6(d). The interference terms $j_x(\mu\nu)$ between orbitals of proton $\pi^2 i_{13/2} f_{7/2}$ pairs are denoted by black solid lines, other interference terms are denoted by black dotted lines. The total interference term from all the proton $\pi^2 i_{13/2} f_{7/2}$ pairs are denoted by olive dashed lines.

It can be seen clearly that the upbendings at $\hbar\omega \approx 0.25$ MeV in the parity-doublet bands in ^{237}U are mainly due to the suddenly gained alignment of protons occupying orbital $\pi 1/2$ $(f_{7/2})$ and high-j intruder orbitals $\pi 3/2$ $(i_{13/2})$ and $\pi 5/2$ $(i_{13/2})$. As shown in Fig. 6(c), the interference terms between $\pi^2 i_{13/2} f_{7/2}$ pairs play a very important role in the sharp increased alignment. For ^{239}Pu, there is little contribution from the interference terms $j_x(\mu\nu)$ from $\pi^2 i_{13/2} f_{7/2}$ pairs at $\hbar\omega < 0.20$ MeV, which decreases slightly at $\hbar\omega > 0.20$ MeV. Therefore, the angular momentum alignments of the parity-doublet rotational bands in ^{239}Pu are quite plain. According to the discussion above, the interference terms of proton octupole correlation pairs of $\pi^2 i_{13/2} f_{7/2}$ play a key role in the rotational properties in the rotational bands between ^{237}U and ^{239}Pu.

D. Simplex splittings in parity-doublet bands of ^{237}U and ^{239}Pu

From Figs. 3(a) and 3(b), one can see that the kinematic moments of inertia and their variations with rotational frequency are very different between $s = +i$ and $s = -i$ bands for ^{237}U. There is a simplex splitting occurs at low rotational frequency ($\hbar\omega < 0.10$ MeV) region. The similar phenomenon occurs in the parity-doublet rotational bands in ^{239}Pu in Figs. 3(c) and 3(d). These simplex splittings in the parity-doublet rotational bands of ^{237}U and ^{239}Pu can be understood from the behavior of the unpaired neutron $\nu 1/2$ $(d_{5/2})$ orbital.

As it shows in Figs. 5(a)–5(d) that the neutron occupation probability in simplex $s = +i$ and $s = -i$ bands for both ^{237}U and ^{239}Pu are very similar. The neutron $\nu 1/2$ orbital is half occupied ($n_\mu \approx 1$), and other neutron orbitals are nearly full occupied ($n_\mu \approx 2$) or empty ($n_\mu \approx 0$). The contributions of neutrons to the moments of inertia $J^{(1)}$ in the parity-doublet bands in ^{237}U and ^{239}Pu are shown in Fig. 7, in which the contributions from the diagonal and off-diagonal parts in the $s = +i$ and $s = -i$ bands are presented in Figs. 7(a) and 7(b), respectively. It can be seen clearly that the simplex splittings in the moments of inertia mainly come from the contributions of the diagonal part.

The diagonal parts $J^{(1)}$ of contribution from each neutron orbitals near the Fermi surface for the parity-doublet rotational bands in ^{237}U and ^{239}Pu are presented in Figs. 7(c) and 7(d). It can be seen that the contribution of each simplex doublet is almost same to each other except for the $\nu 1/2$ $(d_{5/2})$ orbital, which shows significant splittings at $\hbar\omega < 0.10$ MeV. It clearly shows that the simplex splittings of $J^{(1)}$ at $\hbar\omega < 0.10$ MeV for the parity-doublet bands in ^{237}U and ^{239}Pu come from the splitting of the contribution of $\nu 1/2$ $(d_{5/2})$ orbitals.

IV. SUMMARY

The parity-doublet rotational bands in odd-A isotones ^{237}U and ^{239}Pu are investigated by using the cranked shell model with the pairing correlation treated by a particle-number-conserving method, in which octupole deformation are taken into account in reflection-asymmetric nuclear system. The experimental moments of inertia and alignments versus the rotational frequency $\hbar\omega$ are reproduced very well by the PNC-CSM calculations. The microscopic mechanism of the distinct difference of rotational behaviors between the bands in ^{237}U and ^{239}Pu, and simplex splittings in the parity-doublet bands for both of ^{237}U and ^{239}Pu are explained.

Sharp upbendings of the moments of inertia $J^{(1)}$ occur at $\hbar\omega \approx 0.25$ MeV in the parity-doublet bands in ^{237}U whereas

$J^{(1)}$ is quite plain during the whole observed frequency for ^{239}Pu. This is due to the contribution of the alignments from nucleon occupying the octupole-correlation pairs of $\pi^2 i_{13/2} f_{7/2}$. The upbendings of the parity-doublet bands in ^{237}U are due to the alignments of the interference terms of protons occupying the $\pi f_{7/2}$ ($\Omega = 1/2$) and the high-j intruder $\pi i_{13/2}$ ($\Omega = 1/2, 3/2$) orbitals while it contributes a little to the parity-doublet bands in ^{239}Pu.

There are splittings of the simplex partner bands at $\hbar\omega < 0.10$ MeV of the parity-doublet bands in both ^{237}U and ^{239}Pu. It is found that the simplex splittings between the $s = +i$ and $s = -i$ rotational bands result from the contributions of alignment of neutron occupying the $\nu 1/2$ ($d_{5/2}$) orbital.

ACKNOWLEDGMENT

This work is supported by the National Natural Science Foundation of China (Grants No. U2032138 and No. 11775112).

[1] S. K. Saha, M. J. Maynard, B. C. Robertson, A. B. McDonald, and E. D. Earle, Phys. Rev. C **21**, 2322 (1980).
[2] P. C. Sood and R. K. Sheline, Phys. Rev. C **40**, 1530 (1989).
[3] V. Grafen, B. Ackermann, H. Baltzer, T. Bihn, C. Günther, J. deBoer, N. Gollwitzer, G. Graw, R. Hertenberger, H. Kader, A. Levon, and A. Lösch, Phys. Rev. C **44**, R1728 (1991).
[4] W. Reviol, D. G. Sarantites, C. J. Chiara, M. Montero, R. V. F. Janssens, M. P. Carpenter, T. L. Khoo, T. Lauritsen, C. J. Lister, D. Seweryniak, S. Zhu, O. L. Pechenaya, and S. G. Frauendorf, Phys. Rev. C **80**, 011304(R) (2009).
[5] I. Ahmad and P. A. Butler, Annu. Rev. Nucl. Part. Sci. **43**, 71 (1993).
[6] S. Aberg, H. Flocard, and W. Nazarewicz, Annu. Rev. Nucl. Part. Sci. **40**, 439 (1990).
[7] P. Butler and W. Nazarewicz, Rev. Mod. Phys. **68**, 349 (1996).
[8] I. Ahmad, J. E. Gindler, R. R. Betts, R. R. Chasman, and A. M. Friedman, Phys. Rev. Lett. **49**, 1758 (1982).
[9] H. E. Martz, R. K. Sheline, R. G. Lanier, R. W. Hoff, G. L. Struble, D. J. Decman, D. G. Burke, R. R. Chasman, and R. A. Naumann, Phys. Rev. C **37**, 1407 (1988).
[10] M. W. Drigert and J. A. Cizewski, Phys. Rev. C **31**, 1977 (1985).
[11] E. Parr, J. F. Smith, P. T. Greenlees, P. A. Butler, K. Auranen, R. Chapman, D. M. Cox, D. M. Cullen, L. P. Gaffney, T. Grahn, E. T. Gregor, L. Grocutt, A. Herzáň, R.-D. Herzberg, D. Hodge, U. Jakobsson, R. Julin, S. Juutinen, J. M. Keatings, J. Konki, M. Leino, P. P. McKee, C. McPeake, D. Mengoni, A. K. Mistry, B. S. Nara Singh, G. G. O'Neill, J. Pakarinen, P. Papadakis, J. Partanen, P. Peura, P. Rahkila, P. Ruotsalainen, M. Sandzelius, J. Sarén, M. Scheck, C. Scholey, M. Siciliano, M. Smolen, J. Sorri, P. Spagnoletti, K. M. Spohr, S. Stolze, M. J. Taylor, and J. Uusitalo, Phys. Rev. C **105**, 034303 (2022).
[12] I. Ahmad, R. R. Chasman, J. E. Gindler, and A. M. Friedman, Phys. Rev. Lett. **52**, 503 (1984).
[13] C. F. Liang, P. Paris, J. Kvasil, and R. K. Sheline, Phys. Rev. C **44**, 676 (1991).
[14] G. Ardisson, J. Gasparro, V. Barci, and R. K. Sheline, Phys. Rev. C **62**, 064306 (2000).
[15] R. K. Sheline, C. F. Liang, P. Paris, J. Kvasil, and D. Nosek, Phys. Rev. C **51**, 1708 (1995).
[16] W. Reviol, R. V. F. Janssens, S. Frauendorf, D. G. Sarantites, M. P. Carpenter, X. Chen, C. J. Chiara, D. J. Hartley, K. Hauschild, T. Lauritsen, A. Lopez-Martens, M. Montero, O. L. Pechenaya, D. Seweryniak, J. B. Snyder, and S. Zhu, Phys. Rev. C **90**, 044318 (2014).
[17] M. Dahlinger, E. Kankeleit, D. Habs, D. Schwalm, B. Schwartz, R. Simon, J. Burrows, and P. Butler, Nucl. Phys. A **484**, 337 (1988).
[18] I. Wiedenhöver, R. V. F. Janssens, G. Hackman, I. Ahmad, J. P. Greene, H. Amro, P. K. Bhattacharyya, M. P. Carpenter, P. Chowdhury, J. Cizewski, D. Cline, T. L. Khoo, T. Lauritsen, C. J. Lister, A. O. Macchiavelli, D. T. Nisius, P. Reiter, E. H. Seabury, D. Seweryniak, S. Siem, A. Sonzogni, J. Uusitalo, and C. Y. Wu, Phys. Rev. Lett. **83**, 2143 (1999).
[19] S. Zhu, R. Janssens, G. Lane, I. Wiedenhöver, M. Carpenter, I. Ahmad, A. Byrne, P. Chowdhury, D. Cline, A. Deacon *et al.*, Phys. Lett. B **618**, 51 (2005).
[20] M. Bender, P.-H. Heenen, and P. Bonche, Phys. Rev. C **70**, 054304 (2004).
[21] L. M. Robledo and G. F. Bertsch, Phys. Rev. C **84**, 054302 (2011).
[22] W. Zhang, Z. P. Li, S. Q. Zhang, and J. Meng, Phys. Rev. C **81**, 034302 (2010).
[23] H. Ganev, V. P. Garistov, and A. I. Georgieva, Phys. Rev. C **69**, 014305 (2004).
[24] A. A. Solnyshkin, V. P. Garistov, A. Georgieva, H. Ganev, and V. V. Burov, Phys. Rev. C **72**, 064321 (2005).
[25] X. C. Chen, J. Zhao, C. Xu, H. Hua, T. M. Shneidman, S. G. Zhou, X. G. Wu, X. Q. Li, S. Q. Zhang, Z. H. Li, W. Y. Liang, J. Meng, F. R. Xu, B. Qi, Y. L. Ye, D. X. Jiang, Y. Y. Cheng, C. He, J. J. Sun, R. Han, C. Y. Niu, C. G. Li, P. J. Li, C. G. Wang, H. Y. Wu, Z. H. Li, H. Zhou, S. P. Hu, H. Q. Zhang, G. S. Li, C. Y. He, Y. Zheng, C. B. Li, H. W. Li, Y. H. Wu, P. W. Luo, and J. Zhong, Phys. Rev. C **94**, 021301(R) (2016).
[26] D. S. Delion, R. J. Liotta, P. Schuck, A. Astier, and M.-G. Porquet, Phys. Rev. C **85**, 064306 (2012).
[27] M. Warda and L. M. Robledo, Phys. Rev. C **84**, 044608 (2011).
[28] M. Elvers, S. Pascu, T. Ahmed, T. Ahn, V. Anagnostatou, N. Cooper, C. Deng, J. Endres, P. Goddard, A. Heinz, G. Ilie, E. Jiang, C. Küppersbusch, D. Radeck, D. Savran, N. Shenkov, V. Werner, and A. Zilges, Phys. Rev. C **84**, 054323 (2011).
[29] A. Dobrowolski, K. Mazurek, and A. Góźdź, Phys. Rev. C **97**, 024321 (2018).
[30] P. G. Bizzeti and A. M. Bizzeti-Sona, Phys. Rev. C **81**, 034320 (2010).
[31] Y. S. Chen and Z. C. Gao, Phys. Rev. C **63**, 014314 (2000).
[32] Z.-C. Gao, M. Horoi, Y. S. Chen, Y. J. Chen, and Tuya, Phys. Rev. C **83**, 057303 (2011).
[33] Z.-C. Gao, Y. Sun, and Y.-S. Chen, Phys. Rev. C **74**, 054303 (2006).
[34] H. Hübel, A. Byrne, S. Ogaza, A. Stuchbery, G. Dracoulis, and M. Guttormsen, Nucl. Phys. A **453**, 316 (1986).
[35] R. Bengtsson, S. Frauendorf, and F.-R. May, At. Data Nucl. Data Tables **35**, 15 (1986).

[36] P.-H. Heenen, J. Skalski, P. Bonche, and H. Flocard, Phys. Rev. C **50**, 802 (1994).
[37] W. Nazarewicz and P. Olanders, Nucl. Phys. A **441**, 420 (1985).
[38] X.-T. He and Y.-C. Li, Phys. Rev. C **102**, 064328 (2020).
[39] J. Y. Zeng, T. H. Jin, and Z. J. Zhao, Phys. Rev. C **50**, 1388 (1994).
[40] Z.-H. Zhang, Y.-A. Lei, and J.-Y. Zeng, Phys. Rev. C **80**, 034313 (2009).
[41] X.-T. He, S.-Y. Yu, J.-Y. Zeng, and E. Zhao, Nucl. Phys. A **760**, 263 (2005).
[42] J.-Y. Zeng and T.-S. Cheng, Nucl. Phys. A **405**, 1 (1983).
[43] S. X. Liu, J. Y. Zeng, and E. G. Zhao, Phys. Rev. C **66**, 024320 (2002).
[44] Z.-H. Zhang, Nucl. Phys. A **949**, 22 (2016).
[45] A. Bohr and B. R. Mottelson, *Nuclear Structure*, Vol. II (Benjamin, New York, 1975).
[46] R. Jolos, Nucl. Phys. A **587**, 377 (1995).
[47] Z.-H. Zhang, X.-T. He, J.-Y. Zeng, E.-G. Zhao, and S.-G. Zhou, Phys. Rev. C **85**, 014324 (2012).
[48] M. Basunia, Nucl. Data Sheets **107**, 2323 (2006).
[49] E. Browne and J. Tuli, Nucl. Data Sheets **122**, 293 (2014).